Properties of Additively Manufactured Soft and Hard Magnetic Cores for Electrical Machines: Methods and Materials − A Review

Akbar Mohammadi Ajamloo, *Graduate Student Member, IEEE,* Mohamed N. Ibrahim, *Senior Member, IEEE,* and Peter Sergeant, *Senior Member, IEEE*

***Abstract*—Additive Manufacturing (AM) is an emerging topic in the field of electrical machines (EMs), offering the potential to overcome challenges imposed by conventional manufacturing methods. This paper provides an overview of various AM methods and materials used to manufacture soft and hard magnetic cores for EMs, with a particular focus on their multi-physics properties. Since each AM method involves unique processes—such as particle bonding, melting, or sintering—the resulting microstructural properties of the printed cores differ, leading to varied multi-physics characteristics that require in-depth study. The paper outlines both the benefits and challenges associated with AM techniques and materials. Importantly, it explores the detailed properties of Fe-Si and Fe-Co soft magnetic cores as well as hard magnetic cores including NdFeB, ferrite, and alnico printed through different AM methods, comparing them to traditional laminations and commercial hard magnets.**

***Index Terms*—3D printing, additive manufacturing, binder jetting, directed energy deposition, electrical machine, laser powder bed fusion, multi-physics properties, magnetic core.**

I. INTRODUCTION

ADDITIVE Manufacturing (AM), defined as a process of joining materials to make parts from 3D model data, usually layer upon layer, has received widespread acceptance in various applications. AM offers significant advantages including rapid prototyping, streamlined manufacturing, reduced material waste, enhanced design flexibility, and innovative material utilization over traditional methods [1].

Application of AM in Electrical Machines (EMs) is an emerging topic in the field of EMs which has been employed for all main components of EMs. Maturity of the application of AM in different EM components varies significantly, as shown in Fig. 1, ranging from early research for permanent magnets (PMs) to industry level for heat exchanger and windings. Currently, the additively manufactured copper windings are printed with near full density, exhibiting DC electrical resistivity ranging from 96% to 102% of International Annealed Copper Standard [2, 3]. AM unlocks

Akbar Mohammadi Ajamloo, Mohamed N.Ibrahim, and Peter Sergeant are with the Department of Electromechanical, Systems, and Metal Engineering, Ghent University, 9052 Gent, Belgium, also with FlandersMake@UGent—corelab MIRO, 3001 Leuven, Belgium. Mohamed N.Ibrahim is also with the Department of Electrical Engineering, Kafrelshiekh University, 33511 Kafr el-Sheikh, Egypt (email: Akbar.MohammadiAjamloo@ugent.be; Mohamed.Ibrahim@ugent.be; Peter.Sergeant@ugent.be).

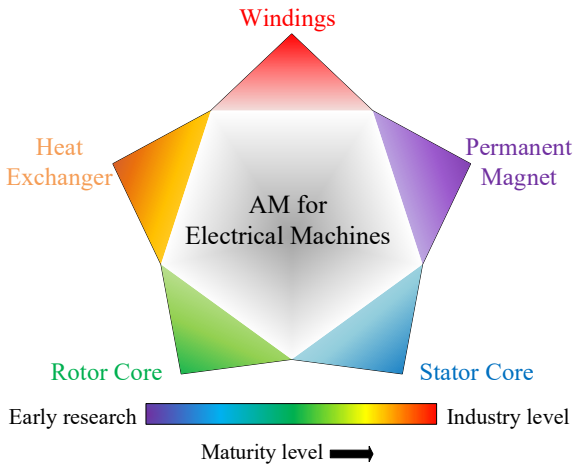

Fig. 1. Maturity overview of application of additive manufacturing in various components of electrical machines.

new possibilities for winding design featuring lower ac loss [4, 5], higher fill factor [6], and more advanced cooling system [7-10] compared to conventionally manufactured windings.

Soft magnetic cores manufactured through AM are currently in the developmental stage, and they have been utilized for both stator and rotor cores of EMs. Unlike conventional laminated cores, which have limitations in the design freedom of core geometry within a 2D plane, AM allows for the creation of intricate 3D core designs. This capability enables a higher degree of freedom in the design of EMs, resulting in enhanced characteristics and performance. In this regard, an additively manufactured stator for axial flux PM machine (AFPM) was proposed in [11, 12], offering around 4% to 7% higher torque density compared to conventional AFPM. A conical air gap machine was introduced in [13], presenting two-times power density compared to its conventional counterpart. New PM rotor core designs were presented in [14-16], exhibiting improvements in certain aspects like, material utilization, torque rating, and thermal performance. Ability to increase the silicon (Si) content in iron-silicon (Fe-Si) cores to the optimal value of 6.5% is another advantage of 3D printed cores over conventional laminated cores. In conventional laminations, increasing the silicon content beyond 3.5% is limited due to highly brittle nature of high silicon steel sheets. In contrast, AM allows for the successful production of soft magnetic Fe-6.5wt%Si cores, showcasing improved electromagnetic

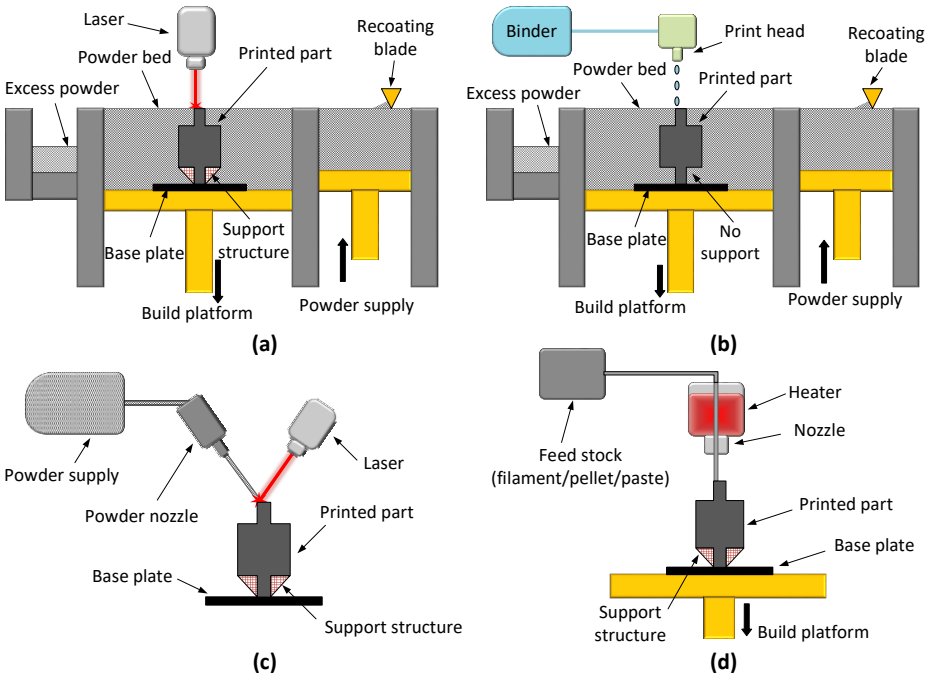

Fig.2. Common AM methods in printing of soft and hard magnetic cores. (a) LPBF, (b) BJ, (c) DED, (d) MEX.

characteristics compared to their conventional laminated counterparts. Presently, the utilization of AM in stator cores is constrained by the difficulties associated with mitigating eddy current losses. On the other hand, the manufacturing of rotor cores through AM has progressed further, benefiting from a quasi-DC magnetic field that induces manageable eddy currents [17]. AM also opens-up a unique opportunity in manufacturing the rotor of high-speed synchronous reluctance motors (SynRMs) through muti-material 3D printing. This approach has been implemented in [18, 19], where the rotor flux carriers are printed with a magnetic material (e.g. Fe-Si) while the flux barriers are printed simultaneously using a non-magnetic metal. This approach enhances the mechanical strength of high-speed rotors compared to traditional laminated designs with hollow flux barriers.

Hard magnetic cores, also referred to as PMs, are nowadays extensively used in EM applications. PM machines have become superior to other types of EMs due to their high power density and efficiency, which are made possible by the use of highly energy-dense rare-earth PMs. However, the significant cost of rare-earth PMs, along with market instability, limited availability of resources, and the substantial environmental damage caused by their mining, has led to serious concerns regarding the widespread use of PM machines. Consequently, the efficient utilization of rare-earth PMs has become a major focus in the industry and academia [20].

Conventional methods for manufacturing PMs, such as sintering and bonding, have certain limitations. Sintering is the most widely used method, known for producing highly dense PMs with desirable magnetic properties. However, this technique often requires significant post-machining, leading to waste of up to 30% of valuable rare-earth materials [21]. Additionally, this method is restricted to creating simple magnet shapes. In contrast, bonding techniques can produce more complex shapes compared to sintering, and they generate minimal material waste since they do not require post-machining. However, the magnetic properties of bonded magnets are considerably inferior to those of sintered magnets due to the use of polymer materials in the bonding process. In this context, AM emerges as a promising alternative to conventional sintering and bonding techniques for producing PMs. AM enables the production of PMs without the need for post-machining. Additionally, AM offers the potential for manufacturing recyclable rare-earth magnets and producing new rare-earth magnets from recycled ones [22, 23]. Moreover, AM is capable of creating highly complex PM geometries as in [24]. This freedom in design can unlock significant potential for optimizing the PM machines with specific objectives, such as minimizing the volume of PM used. For instance, in [25], cold spray AM has been employed to directly print sinusoidal petal-shaped magnets on the rotor surface. This approach resulted in a reduced volume of PM utilized, reduced torque ripple, and eliminated magnet assembly steps. In addition to enabling complex shapes, AM results in near-zero material waste, as it eliminates the need for post-machining. Furthermore, AM provides potential for precise control of grain texture, enabling the tailoring of isotropic and non-isotropic properties of the material [26, 27].

The conference version of this work [28], partially addressed the topic of 3D printing of soft magnetic cores. In this extended version, the scope is significantly expanded by introducing a comprehensive review of 3D printed hard magnetic cores. Additionally, the study on soft magnetic cores has been enhanced by investigating more literatures and providing complementary discussions to fully explore the topic. The existing literature review papers on AM of EM components mainly focused on the design freedom and achievable complex 3D printed components such as windings, heat exchangers, and magnetic cores. However, the multi-physics properties of printed soft and hard magnetic cores, as well as the impact of printing methods and materials on their

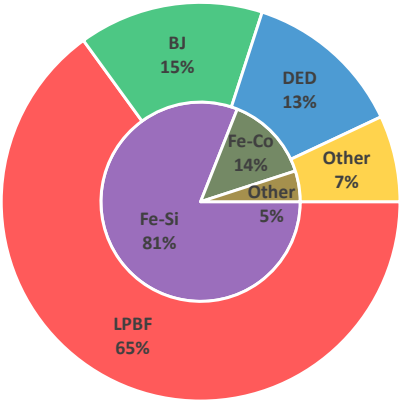

Fig. 3. Distribution of utilized AM methods and materials for 3D printing of soft magnetic cores in the literature (excluding hard magnetic cores).

performance, are either overlooked or not explored in sufficient depth. This is particularly critical because the distinct fusion processes associated with each method, combined with the use of different materials, lead to variations in the microstructural properties of the printed cores. These variations result in diverse multi-physics characteristics that require in-depth investigation which can guide the selection of the appropriate printing method and material and their specific considerations for printing EM component. The current review paper however fully dedicates its entire scope to addressing these gaps. It provides a comprehensive review of current literature, categorizing studies based on the AM methods and materials used and offering insights into the multi-physics characteristics of 3D printed soft and hard magnetic cores for EMs with respect to their commercial counterparts.

II. AM Methods and Materials for Iron Cores

A. AM Methods

In the context of 3D printed metallic parts, four widely employed printing methods are laser powder bed fusion (LPBF), binder jetting (BJ), directed energy deposition (DED), and material extrusion (MEX). The operational principles of these methods are illustrated in Fig. 2. As evident from Fig. 2 (a) and (b), the printing operations of LPBF and BJ rely on utilizing a powder bed, where the printed components are submerged during the layer-by-layer printing process. The key distinction between LPBF and BJ lies in the fusion method. In LPBF, the powder is fused through the thermal energy of the laser beam, whereas in BJ, the powders are fused through a chemical binding agent. When the fusion process for one layer is finished, the build platform is lowered, and a new layer of raw powder is spread above the previous layer by a recoating blade. This process is repeated until the whole 3D part is printed. In DED, laser energy and raw powder are deposited concurrently, either through common or separate nozzles for the laser beam and powder stream. In this process, the printed part remains stationary while the nozzle undergoes 3D motion. In MEX, the feedstock consists of a mixture of metal and thermoplastic material, which can be in the form of filament, pellets, or paste. This feedstock is fed into the nozzle, where it is heated and melted in a controlled

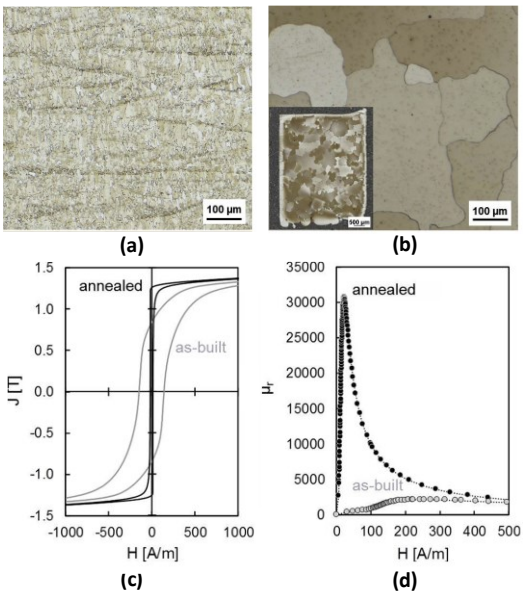

Fig. 4. Effect of heat treatment (annealing for 1 hour at 1150 °C) on microstructure and magnetic properties of 3D printed Fe-6.7wt%Si core. Grain size in (a) as-built and (b) heat treated states. DC measurement of (c) J-H curves and (d) maximum relative permeabilities (μ_r) [29].

manner. The molten material is then deposited onto the build platform, typically in a 2D plane. After each layer is deposited, the build platform is lowered to allow for the deposition of the next layer on top of the previous one.

Due to the thermal fusion of raw powder in LPBF and DED, supporting structures are essential. Without them, parts may curl upwards as internal stresses accumulate during the thermal fusing process. Following the completion of printing, a suitable heat treatment procedure must be employed.

Within the domain of AM for soft magnetic cores used in EMs, various printing methods have been adopted in the literature. As illustrated in Fig. 3, LPBF stands out as the predominant method, accounting for approximately 65% of the relevant literature which is due to its advanced maturity compared to other AM methods. BJ and DED have been employed in approximately 15% and 13% of cases, respectively. The remaining 7% encompasses other types of 3D printing methods including MEX, screen printing, and cold spray [30]. In the context of printing soft magnetic cores, this paper focuses on three main AM methods: LPBF, BJ and DED. The differences in the fusion processes among these methods result in distinct microstructural properties of the printed cores, leading to varied multi-physics properties. Consequently, a detailed investigation is necessary to thoroughly understand and analyze these variations.

B. Heat Treatment and Materials

Heat treatment can be regarded as the most essential post-processing procedure for the 3D printed parts, particularly in alleviating internal stress induced by thermal fusion in LPBF and DED methods. In the case of BJ process, the proper heat treatment results in the removal of binding agent and densification of the metallic phase in the printed part. Apart from its mechanical benefits, the adoption of proper heat

TABLE I
EFFECT OF HEAT TREATMENT ON MAGNETIC PROPERTIES OF SOFT MAGNETIC CORES

Core material	Maximum relative permeability, μ_r		Coercivity, H_c (A/m)		Ref.
	AF	*HT*	*AF*	*HT*	
Fe-Si	590	3300	357	317	[31]
	797	7393	165	35	[32]
	1400	8900	203	52	[33]
	3220	28900	205	41	[34]
	2150	31000	145	16	[29]
Fe-Co-V	518	1615	995	401	[35]
	503	5008	1417	450	[36]
	315	8197	1394	112	[37]
	307	17000	1344	52	[38]

treatment methods is imperative to attain desirable electromagnetic characteristics. The non-heat-treated part which is referred to as " as fabricated " (AF) part exhibit semi-soft magnetic characteristics such as low permeability and high coercivity value. The poor electromagnetic characteristics of AF parts are mainly attributed to increased internal stresses, small grain size, and non-homogenized microstructure caused by the high cooling rates during the printing process [37, 39]. Heat treatment plays a crucial role in enhancing the magnetic properties of the material by relieving internal stresses, increasing grain size, and homogenizing the microstructure through the recrystallization process. Figure 4 illustrates the microstructure and magnetic properties of 3D printed Fe-6.7wt%Si cores before and after heat treatment [29]. It is observed that heat treatment significantly improves the microstructure (grain enlargement) resulting in a substantial increase in relative permeability, decrease in coercivity and reduced hysteresis loss. A comparison of magnetic characteristics between the AF and heat-treated (HT) states for 3D printed cores is presented in Table I. Remarkably, the maximum permeability of HT parts can reach up to 15 times that of the AF state for Fe-Si cores. In the case of HT iron-cobalt-vanadium (Fe-Co-V) cores, the maximum permeability can increase up to 55 times compared to the AF state. Also, the adoption of heat treatments significantly reduces coercivity of the printed cores, leading to a notable decrease in hysteresis loss. It should be noted that while heat treatment is essential for enhancing the magnetic properties of printed soft magnetic cores, it alone does not ensure the attainment of optimal characteristics. This is because various printing parameters, including laser power, laser speed, layer thickness, and scanning pattern significantly influence the microstructure and thereby electromagnetic properties of the printed cores. By fine-tuning these printing parameters, it is possible to achieve significantly increased permeability, along with reduced coercivity and core losses, as presented in [40-42].

Fe-Si is the most prominent commercial alloy in EM application among all soft magnetic alloys, owing to its relatively high resistivity, high permeability, and acceptable magnetic flux density, all achieved at a low price. Successful production of Fe-6.5wt%Si laminations through cold rolling is not feasible due to its extremely low workability. But it is currently commercially manufactured via a chemical vapor deposition (CVD) method and is marketed as JNEX Super Core [43]. However, the CVD process has certain drawbacks, including its high cost and significant environmental impact due to the use of the harmful $SiCl_4$. Fortunately, metal AM avoids the high stress during printing, thereby enables successful manufacturing of Fe-6.5wt%Si cores. Fe-Co alloys are another soft magnetic materials that can be used in EM applications. They are well-known for having the highest maximum magnetic saturation among all engineering soft magnetic materials, reaching up to 2.43 T. Due to the high cost of Co, they are primarily employed in special and volume-constrained applications, such as aerospace, where the lighter weight justifies the higher price. Like Fe-6.5wt%Si, the Fe-Co alloy displays significant brittleness. Typically, around 1.5-2.5% of a metal such as V is incorporated into Fe-Co to enhance its ductility while preserving its electromagnetic properties. However, similar to Fe-6.5wt%Si, the high brittleness and low workability of Fe-Co pose serious challenges when using conventional methods, challenges that can be resolved by leveraging the potential of AM. In the context of soft magnetic alloys used in literatures for 3D printed soft magnetic cores, around 100 studies are investigated. As depicted in Fig. 3, 81% of the studies focus on Fe-Si, around 14% on Fe-Co, and the remaining 5% investigate alternative alloys like Fe-Ni.

III. PROPERTIES OF 3D PRINTED SOFT MAGNETIC CORES

This section explores the electromagnetic and mechanical properties, along with heat treatment details, of 3D printed Fe-Si and Fe-Co-V cores utilizing LPBF, BJ, and DED methods. These constitute more than 90% of the current literature on 3D printed soft magnetic cores for EM application. In terms of electromagnetic properties, the focus is on four attributes: flux density at a field strength of 1000 A/m, coercivity, maximum relative permeability, and DC electrical resistivity. In terms of mechanical characteristics, the focus is on yield strength, defined as the maximum stress a material can endure before undergoing permanent deformation.

A. Soft Magnetic Cores Printed via LPBF

3D printing of Fe-Si magnetic cores with silicon content ranging from 2.9% to 6.9% has been primarily carried out using LPBF, more than any other AM methods. Fe-Si alloys manufactured through 3D printing can be categorized based on their silicon content. Cores with approximately 3.5% silicon are considered to have standard silicon content, aligning with commercial Fe-Si laminations produced through cold rolling, exemplified here by 35A300 [44]. On the other hand, Fe-Si cores with a silicon content of around 6.5% are considered high Si cores, similar to commercial JNEX laminations manufactured through CVD. In this context, the multi-physics properties of both 3D printed Fe-Si cores and commercial laminations are extracted from existing literature and outlined in Table II. It is noticed in both 3D printed and

TABLE II
KEY PROPERTIES OF 3D PRINTED SOFT MAGNETIC CORES BY LASER POWDER BED FUSION (LPBF) COMPARED TO COMMERCIAL LAMINATIONS

	Si%	Flux density (T) at H=1000 A/m	Max. relative permeability, μ_r	Coercivity (A/m)	Electrical resistivity (μΩ.cm)	Heat treatment	Yield strength (MPa)	Ref.
FeSi, Standard Si content	2.9	1.43	3400	116	45.0	2 h at 850 °C	340-400	[45]
	3.0	1.35	4900	~170	-	1 h at 1150 °C	-	[46]
	3.0	1.15	4800	-	-	1 h at 1150 °C	-	[47]
	3.5	1.52	2600	-	-	2 h at 1000 °C	-	[48]
	3.5	1.45	3300	317	-	2 h at 1000 °C	430	[31]
	3.7	1.47	9000	52	-	1 h at 1200 °C	-	[49]
	3.7	1.46	16000	41	56.9	1 h at 1200 °C	420	[50]
FeSi, High Si content	5.5	1.20	3000	102	-	3 h at 1000 °C	615	[51]
	6.5	1.25	2130	43	-	1 h at 500 °C	-	[42]
	6.5	1.35	7000	-	-	2 h at 1200 °C	610	[45]
	6.5	1.20	1500	-	-	at 300 °C	-	[52]
	6.5	1.25	14700	30	-	1 h at 1100 °C	-	[53]
	6.7	1.36	31000	16	82.0	1 h at 1150 °C	-	[29]
	6.9	1.30	4300	49	-	5 h at 700 °C	-	[54]
	6.9	1.32	24000	16	-	1 h at 1150 °C	-	[39]
FeCoV		1.90	1700	357	-	4 h at 1200 °C	-	[45]
		1.50	1450	-	-	4 h at 900 °C	-	[45]
		~1.90	4500	144	-	Two-stage	460	[38]
		2.10	5700	126	-	2 h at 1025 °C	-	[37]
		2.00	~6500	-	43.5	10 h at 820 °C	-	[55]
		2.10	8200	112	-	Two-stage	-	[37]
		2.00	13000	47	47.0	Two-stage	266	[56]
		2.20	17000	52	48.8	Two-stage	265	[38]
		-	-	-	52.0	-	523	[57]
Commercial 35A300	~3.5	1.50	8400	-	51.0	-	400	[44]
Commercial JNEX	6.5	1.30	23000	~17	82.0	-	~600	[43]
Commercial Hiperco 50A		2.20	22000	30-50	40.0	-	200	[58]

commercial Fe-Si cores that a higher Si content generally results in a reduction in coercivity and an increase in electrical resistivity. These are desirable characteristics, as they contribute to reduced hysteresis and eddy current losses in the core, respectively. Furthermore, an increase in the mechanical yield strength is noticed by increasing Si content which is due to the "solid solution strengthening mechanism". The substitution of silicon atoms into the iron lattice creates lattice distortions due to their larger atomic size. These distortions increase resistance to dislocation motion, thereby improving yield strength at the expense of ductility [59].

In [49] and [50], the utilization of Fe-Si with a standard Si content of 3.7% is investigated for the cores of an induction motor and an E-type transformer, respectively. After undergoing a common heat treatment procedure (held at 1200 °C for 1 hour), both cores exhibited superior characteristics compared to the commercial 35A300. Especially in [50], a 90% higher maximum permeability, 12% higher resistivity, and 5% higher yield strength were achieved. In [54], it is shown that establishing correlations between magnetic properties and laser power is a challenging task, primarily due to the simultaneous modification of numerous microstructural features. Factors such as mean grain size, grain distribution, and texture undergo substantial changes. In this complex scenario, porosity and texture emerge as the main drivers influencing magnetic performance. 3D Printing of Fe-6.9wt%Si is explored in [29, 39], achieving superior electromagnetic characteristics with respect to commercial laminations. Particularly in [29], the reported results for 3D printed Fe-6.7wt%Si cores - HT at 1150 °C for 1 hour - reveal a maximum relative permeability of 31000 and electrical resistivity of 82 μΩ.cm. These indicate significantly enhanced properties compared to 35A300 and JNEX laminations, which exhibit a maximum permeability of 8400 and 23000, and resistivity of 51 μΩ.cm and 82 μΩ.cm, respectively.

Electromagnetic and mechanical characteristics of Fe-Co alloy printed by LPBF have been investigated in several studies, with promising results reported. In [37], several Fe-Co sample cores were printed and subjected to various heat treatment scenarios. The most desirable electromagnetic characteristics were achieved for the sample that underwent a two-stage heat treatment process,: first, heat treated at 1027 °C for 2 hours, followed by a second round of heat treatment at 850 °C for 4 hours. In [36], an effective production strategy is presented, utilizing LPBF to achieve the desired mechanical and magnetic properties. The measured results indicated the highest yield strength of 625 MPa, which is more than three times the yield strength of the commercial laminated Hiperco 50A with a composition of 49% Fe, 49% Co, and 2% V [58]. Superior mechanical characteristics and electrical resistivity for the 3D printed Fe-Co cores are also reported in [38, 56]. Notably, in [38], the measured data indicated a 22% higher electrical resistivity and a 33% higher yield strength, all with comparable magnetic characteristics to Hiperco 50A.

B. Soft Magnetic Cores Printed via BJ

In [60], the fabrication of a Fe-6.5wt%Si core using BJ was carried out, with a focus on evaluating the multiphysics characteristics of the printed samples. The measured results reveal a maximum relative permeability and flux density

TABLE III
PROPERTIES OF 3D PRINTED SOFT MAGNETIC CORES BY BINDER JETTING (BJ)

	Si%	Boron content %	Boron particle size (µm)	Flux density (T) at H=1000 A/m	Max. relative permeability, μ_r	Mass density (g/cm^3)	Elec. resistivity (µΩ.cm)	Heat treatment	Yield strength (MPa)	Ref.
FeSi, processed by BJ	6.8	0.25	1.0	0.95	1050	-	-	at 1100 °C	-	[61]
	6.8	0	-	0.80	1100	-	-	at 1200 °C	-	[61]
	6.8	0.25	1.0	0.90	950	-	-	at 1200 °C	-	[61]
	6.8	0.25	1.0	1.10	5200	7.1	-	6 h at 1150 °C	-	[62]
	5	0.25	1.0	1.20	4750	-	-	6 h at 1200 °C	-	[63]
	5	0.25	0.5	1.20	4660	-	-	6 h at 1200 °C	-	[63]
	5	0.25	0.1	1.25	4820	-	-	6 h at 1200 °C	-	[63]
	6.5	0	-	1.00	10500	7.3	98	Multi-stage	430	[60]

TABLE IV
PROPERTIES OF 3D PRINTED SOFT MAGNETIC CORES BY DIRECTED ENERGY DEPOSITION (DED)

	Flux density (T) at H=1000 A/m	Max. relative permeability, μ_r	Heat treatment	Yield strength (MPa)	Reference
FeCoV Processed by DED	1.90	500	AF	-	[35]
	2.15	1700	2 h at 840 °C	-	[35]
	1.10	900	AF	-	[64]
	2.10	12600	4 h at 865 °C	265	[64]
	-	-	at 525 °C	600	[65]
	2.20	6500	Two-stage	-	[66]

(at 1000 A/m) of 10500 and 1 T, respectively. However, these characteristics are notably inferior to the magnetic properties of commercial JNEX. Additionally, the electrical resistivity of the printed core is measured at 98 µΩ.cm, significantly higher than that of commercial JNEX with a resistivity of 82 µΩ.cm, despite a similar material composition. The higher electrical resistivity of the printed core can be attributed to the presentence of porosity, structural defects and non-removed binder in the core structure which also leads to deteriorated magnetic characteristic. The measured mass density of 7.31 g/cm^3 compared to its fully dense state with a mass density of 7.5 g/cm^3, supports the indication of porosity and/or non-removed binder in the printed core. In [63], it was demonstrated that the addition of 0.25% boron (B) to Fe-5wt%Si samples contributes to the reduction of core losses. In this context, experimental characterization of three Fe-Si samples with three different boron particle sizes (1, 0.5, and 0.1 µm) has revealed a nonlinear and somewhat complex relationship between boron particle size and magnetic properties. Nevertheless, the results show a reduction in core losses by almost 10% without a significant change in magnetization properties. In the study presented in [67], the impact of Si and B content on the coercivity and hysteresis loss of Fe-Si cores produced through BJ was investigated. A comparative analysis was conducted between samples containing 3% and 5% Si, with 0.25% B, and those without B. The measured results indicated that the samples with 0.25% B exhibited lower coercivity, reduced hysteresis loss density per electrical cycle, and an increased average grain size. Furthermore, the addition of Si was observed to have a positive effect on the hysteresis loss of printed Fe-Si samples, although the impact was less evident compared to the addition of B at the tested levels. It was also shown that the interaction between the Si and B content on hysteresis loss and grain size is very low. The properties of Fe-Si cores printed via BJ have been gathered from relevant literature and are presented in Table III. Notably, currently there is a lack of reported adequate data on the properties of printed Fe-Co cores using BJ. According to data extracted from the literature, the mass density of the printed Fe-Si cores falls within the range of 6.5 g/cm^3 to 7.3 g/cm^3. This range is notably lower than that of fully dense parts, which typically exhibit a mass density of 7.5 g/cm^3. The observed difference is attributed to the partial diffusion of powder particles, large amount of porosity, and the presence of unremoved binder within the printed part.

Manufacturing Fe-Si cores with satisfying dimensional accuracy using BJ poses a serious challenge. This challenge mainly arises from a substantial shrinkage, reaching up to 20%, occurring after heat treatment [68]. This shrinkage results from the consolidation of the printed powder and the removal of excess binder. While reducing the heat treatment temperature and duration can mitigate shrinkage, such adjustments often come at the expense of deteriorating the mass density and yield strength of the final part. In this regard, it has been demonstrated that the application of Hot Isostatic Pressing (HIP) sintering technology can enhance both the mass density and mechanical strength of printed parts [69]. Additionally, introducing a small quantity of sintering additives, such as B, into the main powder can improve the consolidation process during printing, consequently leading to relatively enhanced mechanical properties [68].

C. Soft Magnetic Cores Printed via DED

Directed Energy Deposition (DED), also known as Laser Engineering Net Shaping (LENS), has been employed in numerous research studies for printing Fe-Co and Fe-Ni soft magnetic cores. In [70], several Fe-Co samples with varying Fe percentages ranging from 30% to 70% were printed using DED. The samples were compared in terms of magnetic saturation, coercivity, and mechanical properties. The findings revealed that the maximum magnetic saturation increased with higher Fe percentages, indicating a positive correlation.

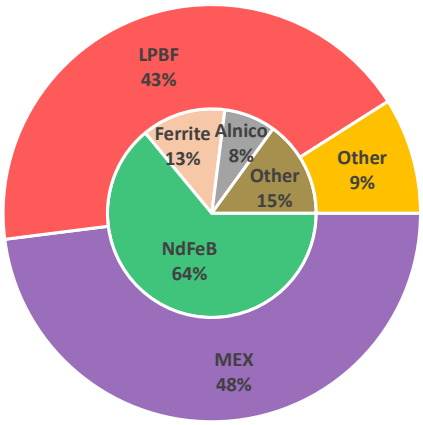

Fig. 5. Distribution of utilized AM methods and materials for 3D printing of hard magnetic cores (PMs) in the literature (soft magnetic cores are excluded).

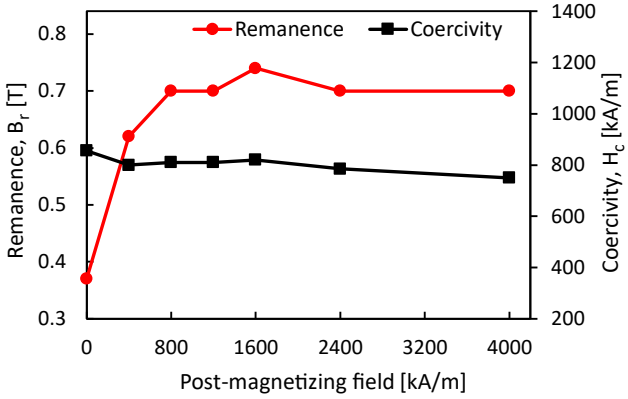

Fig. 6. The effect of post-magnetization on magnetic characteristics of 3D printed PMs (composite of NdFeB + SmFeN + PA 12, printed via MEX) [71].

However, the coercivity exhibited a non-monotonic change with variations in composition. The sample with 55% Fe showed the highest values for both maximum hardness and yield strength among the printed samples. In the study presented in [66], the impact of laser power (ranging from 200 W to 400 W) and heat treatment on the electromagnetic and mechanical characteristics of Fe-Co samples was investigated. A notable trend was observed, indicating a decrease in hardness with an increase in laser power. Additionally, a two-step heat treatment process, consisting of an initial treatment at 950 °C followed by a subsequent treatment at 500 °C, led to a significant reduction in coercivity. In the findings reported in [65], the successful 3D printing of Fe-Co cores is highlighted, showcasing an outstanding balance of high mechanical strength and high ductility. Notably, a remarkable maximum yield strength of approximately 600 MPa was achieved for the heat-treated Fe-Co cores, surpassing the values reported for all 3D printed Fe-Co cores using DED. Furthermore, when compared to the commercial Hiperco, which has a yield strength of 200 MPa, the results indicate an impressive increase of yield strength by around 200%. This suggests a promising approach for overcoming the limitations associated with traditional process metallurgy methods. Research on the 3D printing of soft magnetic cores using DED has mainly focused on Fe-Co cores rather than Fe-Si cores. Regarding this, experimental results from existing literature on the characteristics of 3D printed Fe-Co cores by DED are summarized in Table IV. Specifically, in [64], magnetic test ring samples of Fe-Co were manufactured using DED and subsequently heat-treated at 865 °C for 4 hours. The recorded maximum magnetization saturation falls within the range of 2.3 to 2.4 T, demonstrating compatibility with the commercial Hiperco 50A. However, the lowest achieved coercivity was measured to be around 60 A/m, which was higher than the coercivity of Hiperco 50A. Mechanical test results indicate a yield strength of 265 MPa for the 3D printed samples, representing a 33% increase compared to their commercial counterparts. A clear correlation was established between the initial grain size of the AF Fe-Co cores and the applied printing power, with higher printing power yielding larger grains. Following heat treatment, a noticeable increase in grain size was observed, exhibiting an inverse relationship with laser power; specifically, lower printing power resulted in the largest grain size post-heat treatment. These findings align with anticipated outcomes arising from differences in cooling rates. Increased cooling rates are expected to induce higher residual stresses in the AF samples. Heat treating samples with higher residual stress triggers earlier recrystallization in the heat treatment cycle, allowing more time for grain growth and consequently leading to larger grain sizes post-heat treatment.

IV. 3D Printed Hard Magnetic Cores

In this section, the electromagnetic and mechanical properties of 3D-printed rare-earth and non-rare-earth PMs are investigated and compared to commercial PMs produced via conventional sintering and bonding methods. Over 70 studies on 3D printed PMs have been reviewed and categorized based on the printing method and PM material used. As shown in Fig. 5, MEX and LPBF are the most widely adopted AM methods, representing 48% and 43% of the relevant literature, respectively. The remaining 9% includes DED, BJ, and cold spray techniques. Regarding the PM materials, the studies primarily focused on NdFeB, accounting for 64% of the research. Ferrite magnets comprised 13% of the studies, while the remaining research examined Alnico, SmCo, SmFeN, etc.

A. NdFeB

Among commercial PMs, NdFeB is the most energy-dense and is widely used in high power density EMs. Its widespread use, coupled with its high cost, has made it a dominant focus of research in 3D printing of PMs, as advancements in this area offer significant potential benefits.

Selective laser melting (SLM) and selective laser sintering (SLS), both of which fall under the category of LPBF, are widely used for 3D printing NdFeB magnets. In SLM, NdFeB powder is fully melted using a high-power laser, producing parts with near-theoretical density, which is crucial for achieving high magnetic performance. In contrast, SLS heats the powder just enough to fuse the particles together with the help of a bonding agent, without fully melting the NdFeB powder. SLS is typically used to print polymer-bonded NdFeB magnets by mixing NdFeB powder with a polymer matrix. As a result, NdFeB magnets produced by SLS have lower density compared to those made by SLM, due to the presence of the

polymer, leading to potentially weaker magnetic properties. However, printing NdFeB magnets using SLM requires careful attention to print parameters, as the high temperatures involved in the process can cause oxidation and magnetic degradation of the magnet which is a current challenge in this area. Additionally, the large thermal stresses caused by the rapid heating and cooling rates in SLM can easily lead to cracking in printed NdFeB magnets, which must be carefully managed. In [72], optimized laser parameters and a re-scanning strategy were proposed, resulting in a crack-free NdFeB magnet with high relative density of 96.7% and maximum energy product of 85.9 kJ/m³, achieved by reducing thermal gradients during the printing process. The effect of post-heat treatment and LPBF parameters on the magnetic properties of printed NdFeB magnets was investigated in [73, 74]. The study in [73] examined maximum heat treatment temperatures ranging from 500 °C to 800 °C in 50 °C increments, with a 30-minute hold time, across three sets of printing parameters. The results indicate that the magnetic properties of the magnets can be adjusted through the careful selection of LPBF process parameters and the post-process heat treatment temperature. Magnets with low initial coercivity after printing demonstrated a significant enhancement in coercivity, remanence, and maximum energy product. However, it was also shown that increasing the heat treatment temperature beyond an optimal value led to a significant deterioration of the magnetic properties.

In MEX technique, NdFeB powder is mixed with polymer material and then extruded to print the desired geometry. In this context, the amount of NdFeB powder incorporated into the composite material is an important parameter known as the "loading fraction", the square of which is proportional to the maximum energy product of the PM. The typical loading fraction for 3D printed bonded NdFeB magnets now reaches up to 0.7 by volume, which is comparable to conventional injection molding at the same loading fraction and somewhat lower than the compression molding process, which has a loading fraction of around 0.8 by volume. In the context of 3D printed NdFeB magnets via MEX, the type of polymer material used in the magnet composite significantly influences the magnet's density, printability, and mechanical, thermal, and magnetic properties. Currently, Polyamide 12 (PA 12) is the most commonly used polymer in the literature for 3D printing NdFeB PMs via MEX. In [75], a comparison was made between using PA 12 and thermoplastic polyurethane (TPU) in 3D printed bonded NdFeB magnet. The results showed that using TPU allowed for a higher volume fraction of NdFeB in the printed part, leading to improved magnetic performance, particularly an increase in the maximum energy product from 25.9 kJ/m³ (PA 12) to 47.5 kJ/m³ (TPU). However, the study also revealed that magnets printed with PA 12 exhibited much better mechanical and thermal properties compared to those printed with TPU. Post-magnetizing printed magnets using an external field is a critical step to achieve desirable magnetic properties. In this context, [71] investigated the effect of post-magnetization for a composite of NdFeB + SmFeN + PA 12, fabricated using MEX. The printed magnets were subjected to post-

TABLE V
PROPERTIES OF SOME 3D PRINTED PMS IN THE LITERATURE COMPARED TO COMMERCIAL PMS

Magnet type	Production method	Remanence, B_r [T]	Intrinsic coercivity, H_{cj} [kA/m]	Max. Energy product, $(BH)_{max}$ [kJ/m^3]	Relative volumetric density [%]	Tensile strength [MPa]	Ref
NdFeB	LPBF	0.3	708	15.3	47.4	-	[76]
		0.385	721	24.1	57.7	-	[77]
		0.55	825	-	90	-	[78]
		0.563	516	35.9	90.9	-	[79]
		0.59	695	45	92.1	-	[24]
		0.62	1790	65	>94	-	[80]
		0.65	637	62.8	91	-	[81]
		0.66	725	63	-	-	[73]
		0.7	438	48.1	-	-	[74]
		0.85	718	85.9	96.7	-	[72]
	MEX	0.3	980	-	46.5	-	[82]
		0.37	950	-	52.6	10.4	[83]
		0.5	907	43	63.8	20.4	[84]
		0.51	688	43	63.2	6.6	[85]
		0.58	708	58.1	68.4	-	[86]
		0.72	875	87.5	-	-	[71]
	BJ	0.3	716	-	45.7	-	[87]
		0.31	1345	-	56.6	-	[88]
	Cold spray	0.364	989	-	-	82.4	[89]
		0.49	700	-	-	215	[90]
Commercial NdFeB (bonded)		0.35-0.8	440-1200	22-95	53-82	22-43 (injection molding)	[91, 92]
Commercial NdFeB (sintered)		1.2-1.5	870-950	280-430	~100	~80	[93]
Ferrite	MEX	0.21	245	-	58	39.9	[94]
		0.22	281	-	57	-	[95]
		0.264	196	-	-	-	[96]
		0.383	271	26.3	97	-	[97]
Commercial Ferrite		0.2-0.4	210-360	7-42	70-96	~34	[98]
Alnico	DED	0.81	151	30.8	>99	-	[99]
	LPBF	0.9	108	49.4	-	-	[100]
	DED	0.92	142	47.8	-	-	[101]
Commercial Alnico		0.7-1.35	50-152	34-80	95-99	20-450	[102]

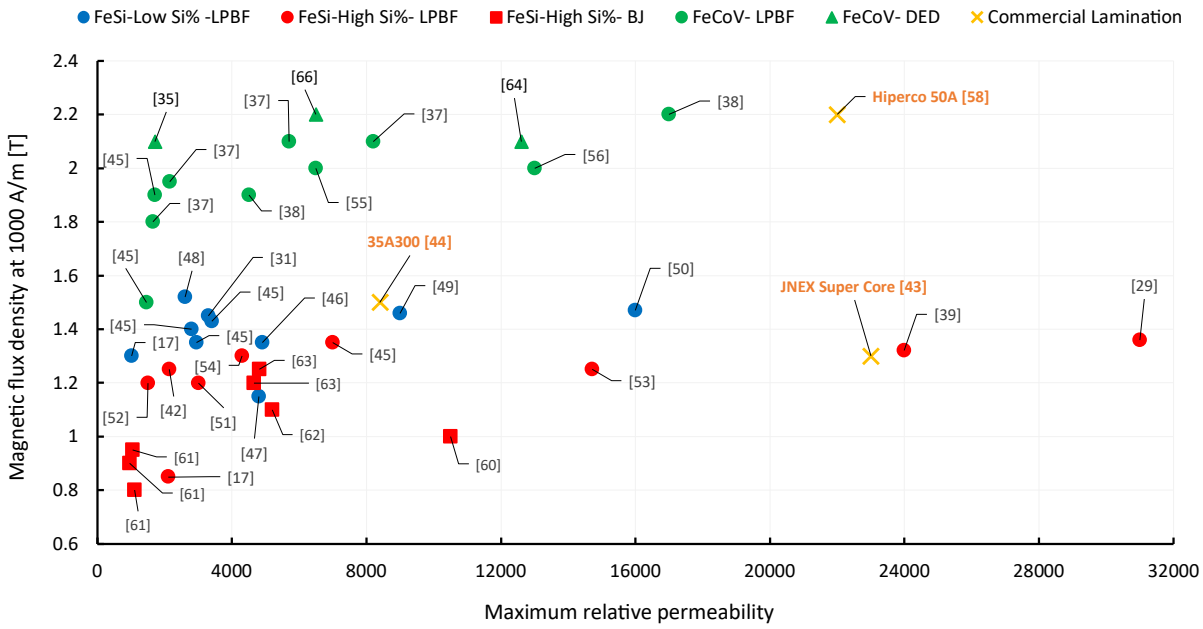

Fig. 7. Magnetic characteristics of Fe-Si and Fe-Co cores printed by different AM techniques, compared with commercial laminations.

magnetization under external fields ranging from 0 to 4,000 kA/m, as illustrated in Fig. 6. The results reveal a substantial increase in remanent flux density, from 0.37 T for the as-printed magnets to over 0.7 T for the post-magnetized ones. Furthermore, the effect of the temperature during the post-magnetization was investigated for temperatures between 25 °C and 257 °C. The study showed that increasing the temperature to a specific value for each applied magnetization field resulted in optimal magnetic properties. However, further increases in temperature led to a deterioration of these properties. It was concluded that post-magnetizing the samples at 1,200 kA/m and 205 °C achieved a maximum energy product of 87.5 kJ/m³, which is a significant improvement compared to the non-post-magnetized sample with maximum energy product of around 24 kJ/m³.

B. Ferrite and Alnico

Ferrite PMs, also known as ceramic magnets, are made from iron oxide combined with another metallic element, such as barium (Ba) or strontium (Sr). Therefore, Ba-ferrite and Sr-ferrite are two widely used types of ceramic PMs, with Sr-ferrite offering superior magnetic properties, making it the preferred choice for more demanding applications. Alnico magnets are another common type of rare-earth-free PMs composed primarily of aluminum, nickel, and cobalt. Although both ferrite and alnico PMs have weaker magnetic properties compared to NdFeB, they offer unique advantages in EM applications due to their low cost, as well as superior thermal stability and corrosion resistance. In the context of 3D printing ferrite and alnico magnets, the low cost of their raw materials shifts the emphasis from minimizing material waste to creating complex geometries with suitable magnetic characteristics. These intricate designs are often challenging or impossible to achieve with conventional manufacturing techniques but can unlock new opportunities for optimal design of EMs through the potential of AM. However, at the current stage of AM's maturity, the focus of literature is to print magnets with magnetic performance comparable to that of commercial magnets. In this regard, the characteristics of some 3D printed ferrite and alnico magnets are listed in Table V and compared to their commercial counterparts. Particularly in [97], a successful 3D printing of Sr-ferrite magnets was reported using material extrusion (MEX). The printed samples achieved 97% of the relative full density with good magnetic characteristics, including a remanence of 0.38 T and an intrinsic coercivity of 271 kA/m, which are comparable to commercial Sr-ferrite magnets produced via injection molding. For alnico magnets, which have much lower coercivity compared to ferrite and NdFeB, maintaining sufficient coercivity in 3D printed alnico magnets is crucial for their applicability in EM applications, where resistance to demagnetization is a key requirement. Among the reported characteristics for 3D printed alnico magnets in the literature, [99-101] reported coercivity values between 100 and 150 kA/m, which are comparable to high-quality commercial alnico magnets as listed in Table V.

V. Comparison and Discussion

This section provides a comparative discussion on the electromagnetic and mechanical properties of 3D printed soft and hard magnetic cores, using different materials and 3D printing methods, with respect to commercial laminations and PMs available in the market. Additionally, the current status and printing capabilities of commercially available 3D printers, and key research directions in this topic are examined and discussed.

A. Soft Magnetic Cores

Figure. 7 illustrates the magnetic flux density of 3D printed soft magnetic cores measured at 1000 A/m versus maximum relative permeability in the HT state. The data are categorized based on material and printing technique, and comparisons are made with three commercial laminations. For Fe-Co cores manufactured by LPBF and DED, the printed cores exhibit magnetic flux density within the same range as commercial

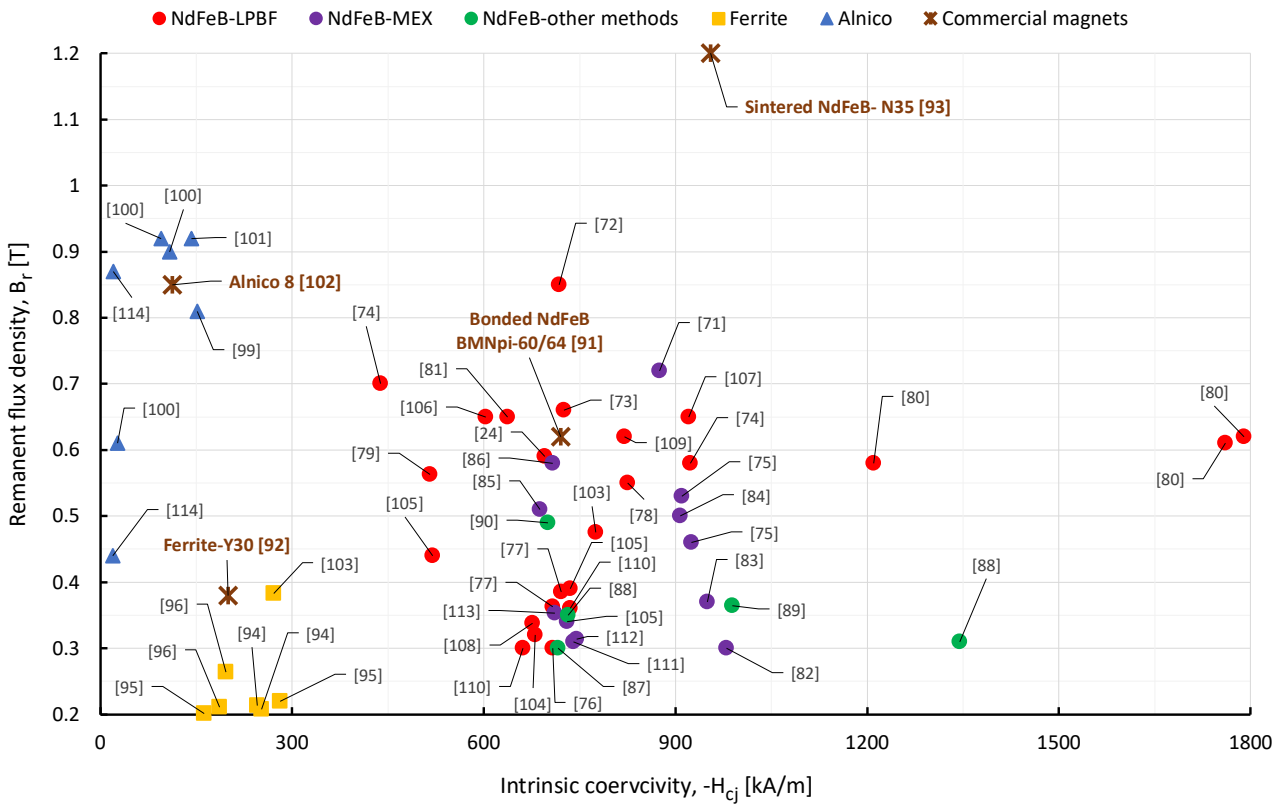

Fig. 8. Remanence and intrinsic coercivity of 3D printed NdFeB [24, 71-90, 103-113], ferrite [94-97], and alnico magnets [99-101, 114] vs commercial PMs.

Hiperco but with noticeably lower maximum permeability. Fe-Si cores with standard Si content demonstrate a similar flux density compared to commercial 35A300. Maximum permeability values reported in the literature generally range from 3400 to 16000, with some cases surpassing the maximum permeability of their commercial counterpart, particularly in [49] and [50]. In the category of Fe-Si cores with high Si content printed by LPBF, a similar trend is observed, with some cases showing considerably enhanced maximum permeability compared to commercial JNEX. In comparison to soft magnetic cores printed by LPBF and DED, those printed by BJ exhibit considerably inferior magnetic characteristics. This may be attributed to the presence of porosity and traces of non-removed binding agent in the material. Additionally, the tradeoff between lowering the heat treatment temperature and shrinkage in binder jetted cores may lead to an improper heat treatment procedure, resulting in deteriorated characteristics. Concerning the electrical resistivity, data from existing literature provided in Tables II, III, and IV suggest that, the 3D printed cores generally exhibit comparable or higher electrical resistivity with respect to commercial laminations. Regarding the mechanical characteristics, the 3D printed cores demonstrate enhanced yield strength in comparison to their commercial counterparts in many reported results as listed in Table II.

Regarding heat treatment, the literature summarized in Tables II, III, and IV indicates that for 3D printed Fe-Si cores fabricated via LPBF, single-stage heat treatment for 1 hour at temperatures ranging from 1100°C to 1200°C yields more favorable magnetic properties. In the case of Fe-Co cores printed via LPBF and DED, a two-stage heat treatment process for 2-4 hours, at temperature between 700°C and 1000°C, achieved more promising results. In the case of BJ, longer holding durations of up to 6 hours or adopting multi-stage heat treatment appear to result in more acceptable magnetic properties for Fe-Si cores. However, there is a notable lack of sufficient studies in the literature regarding the proper heat treatment for obtaining suitable magnetic characteristics in magnetic cores printed via BJ.

B. Hard Magnetic Cores

The remanence and intrinsic coercivity of 3D printed NdFeB, ferrite, and alnico magnets are illustrated in Fig. 8. For 3D printed NdFeB, remanence values typically range from 0.3 T to 0.7 T across most studies, except in [72], where a remanence of 0.85 T was achieved using the LPBF process. Reported coercivity values generally range from 400 kA/m to 1,200 kA/m, except in [80], where high coercivity values of around 1800 kA/m were achieved. It is also observed that NdFeB magnets printed via LPBF generally exhibit better magnetic properties compared to those printed using MEX. This can be attributed to the higher relative density achieved with the LPBF process, which allows for a greater load of NdFeB powder in the printed magnet. Overall, the remanence and coercivity of 3D printed NdFeB magnets are comparable to commercial bonded NdFeB magnets (Table V). However, when compared to commercial sintered NdFeB magnets, which have remanence values of 1.2 T or higher, the 3D printed magnets are significantly weaker. In terms of mechanical strength, the reported data in the literature covers a wide range. However, studies in [90-92] reported printing NdFeB magnets using the cold spray method, achieving higher tensile strength compared to both commercial bonded and sintered NdFeB magnets as listed in Table V.

TABLE VI
SPECIFICATIONS OF SOME COMMERCIAL METAL 3D PRINTERS, CATEGORIZED BY PRINTING METHOD

Printing Method	Printer name	Manufacturer	Laser/nozzle description	Part dimension accuracy	Layer height (µm)	Build volume (mm)	Max. build rate (cm³/h)	Ref.
LPBF	DMP Flex 100	3D Systems	1 laser, 100 W	50 µm	10-100	100×100×90	-	[115]
	XM 200 G2	XACT Metal	2 lasers, 400 W	-	20-100	150×150×150	16	[116]
	HBD 1000Pro	HBD	8 lasers, 500 W	50 µm	20-120	660×660×1250	-	[117]
	SLM 125	Nikon SLM	1 laser, 400 W	-	20-75	125×125×125	25	[118]
	SLM 500	Nikon SLM	4 lasers, 700 W	-	20-90	500×280×365	171	[119]
	FormUp 350	AddUp	4 lasers, 500 W	100 µm	-	350×350×350	-	[120]
	Print Genius 400 XL	Prima Additive	4 lasers, 500 W	-	20-100	430×430×1000	120	[121]
BJ	PX 100	Markforged	1 head, 70400 nozzles	0.5%	42	250×217×186	1000	[122]
	HP Metal Jet S100	HP	6 heads, 63360 nozzles	-	35-140	430×309×140	1990	[123]
	X160 Pro	Desktop Metal	4 heads, 4096 nozzles	-	30-200	800×500×400	3120	[124]
	Production System P-1	Desktop Metal	8 heads, 4096 nozzles	0.5%	30-200	200×100×40	1350	[125]
	Production System P-50	Desktop Metal	8 heads, 16384 nozzles	1.0%	30-200	440×330×250	12000	[125]
DED	Meltio M450	Meltio	1 nozzle, 6 lasers (200 W)	500 µm	-	145×168×390	-	[126]
	Modulo 400	AddUp	1 nozzle, 2000 W laser	200 µm	200-700	650×400×600	150	[127]
	Magic 800	AddUp	1 nozzle, 2000 W laser	200 µm	200-700	1000×1800×1000	130	[128]
	AMDroid	ADDITEC	1 nozzle, 6000 W laser	250 µm	800-1200	1800×1250×1400	500	[129]
MEX	Metal X	Markforged	2 nozzles	500 µm	85-170	300×220×180	-	[130]
	Forge1	Raise3D	2 nozzles	-	100-250	300×300×300	-	[131]
	Studio System 2	Desktop Metal	1 nozzle	-	50-300	300×300×200	-	[132]

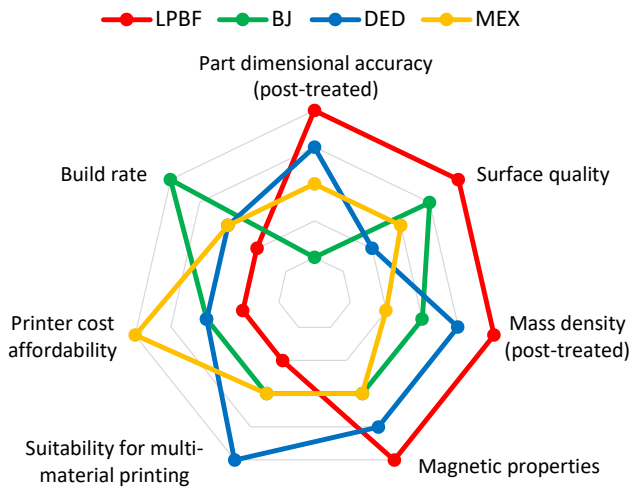

Fig. 9. Comparison of main AM techniques for printing magnetic cores of EMs.

For 3D printed ferrite magnets, the remanence falls within the range of 0.2 T to 0.3 T, which corresponds to low-grade to middle-grade commercial ferrite PMs. However, in [97], ferrite magnets with a remanence of 0.38 T were printed using the MEX method, which are comparable to highest grades of commercial ferrite magnet. For 3D printed alnico PMs, high coercivity values of up to 151 kA/m have been achieved, which is comparable to the highest grades of commercial alnico. However, the remanence in most cases falls between 0.7 T and 0.9 T, corresponding to the middle grades of commercial alnico magnets.

C. Status of AM Methods and Commercial Metal 3D Printers

To provide a clearer perspective on the performance of different 3D printing methods, Table VI presents a list of some commercial metal 3D printers available in the market, categorized by the printing technique utilized, along with their detailed characteristics as declared by their supplier. Furthermore, a comprehensive comparison of the printing techniques in the context of manufacturing magnetic cores are presented in Fig. 9. According to the comparative magnetic characteristics presented in previous parts, LPBF stands out as the commonly used and has demonstrated more promising results overall among the 3D printing methods for producing soft and hard magnetic cores. This can be attributed to the maturity of LPBF technology, which has been continuously developed for over two decades. LPBF-based printers are currently the most suitable choice for high quality metal 3D printing, offering a minimum printing accuracy of 50 µm. The high printing accuracy of the LPBF technique makes it the ideal choice for implementing intricate eddy current loss-limiting patterns in magnetic cores. When applying these patterns to the magnetic cores of EMs, the material filling factor, which directly affects the machine's power rating, should be as high as possible. Achieving this requires minimizing the distance between pattern layers, which is governed by the printing accuracy of the AM method. If the minimum distance between the pattern layers is incompatible with the 3D printer's resolution, the layers may be short-circuited, becoming ineffective in reducing eddy current losses. In this regard, the LPBF technique is considered as the most suitable method for applying eddy current limiting patterns. Furthermore, in LPBF technique, minimum surface roughness of 5 µm Ra is achievable by allowing the adjustment of the layer height down to 10 µm [115]. The resulting parts exhibit near-full density, exceeding 99% of the fully dense part. However, drawbacks include a very low printing speed, typically around 90 cm³/h for medium size printers [133], the necessity for supporting structures, and high printer price.

In contrast, BJ printing technology offers very fast printing speed and eliminates the need for support structures. For instance, in "Production System P-50", the printing speed reaches up to 12,000 cm³/h, making it ideal for high-volume production [125]. Nonetheless, a significant challenge with the BJ is its low dimensional accuracy due to high and not

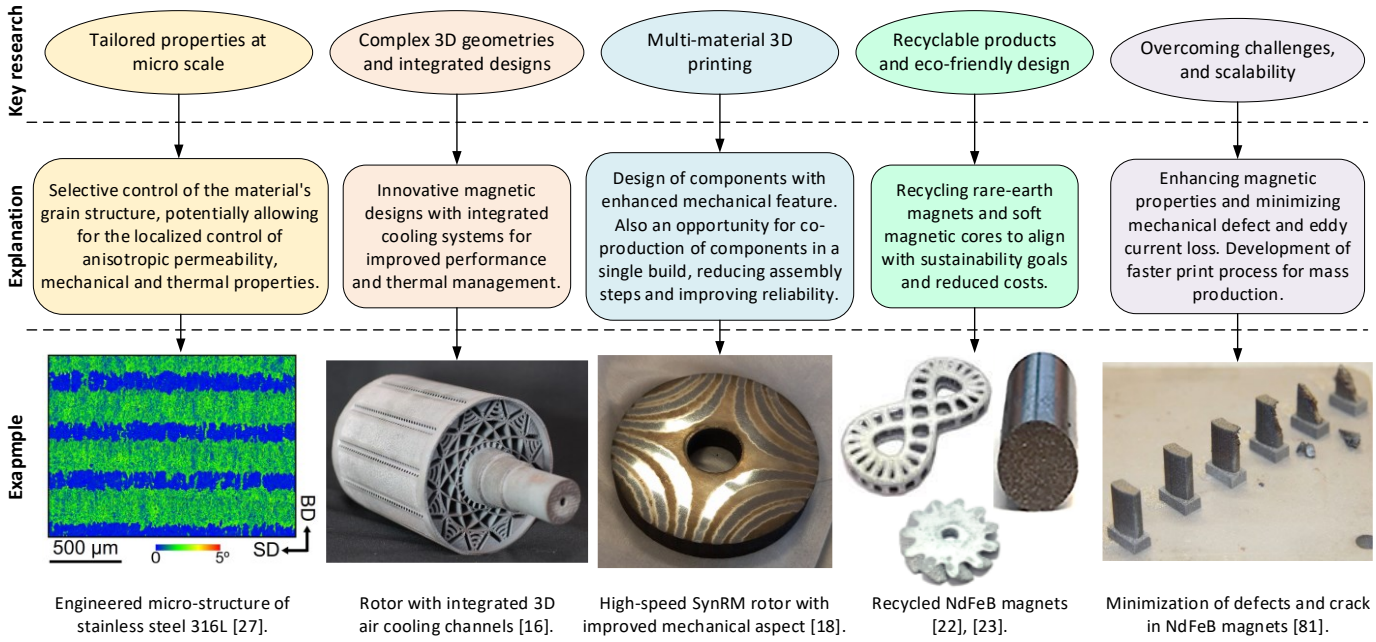

Fig. 10. Ongoing and future research directions in 3D printing of magnetic cores for electrical machine components.

perfectly controllable shrinkage occurred post-printing sintering, which is roughly 20% [68]. Additionally, based on the reviewed literature, iron alloys printed via BJ exhibit very low mass density, typically around 90% of the fully dense part, and also sub-optimal magnetic characteristics.

DED presents advantages such as the ability to print highly-dense parts, with densities in the range of 97% to 99%, and relatively fast build rates of up to 700 cm^3/h. DED-based printers also offer excellent capabilities for multi-material printing. Many DED printers are equipped with multiple material feeds, and their advanced control systems enable the simultaneous mix and deposition of different materials. DED also provides excellent integration with CNC machining in hybrid machines, enabling both additive and subtractive manufacturing in a single setup. Some commercial DED-CNC systems already offer this capability as in [127, 128]. This is particularly useful for repairing worn-out parts, where material is added only in the necessary areas and then precisely machined for a perfect fit. However, DED-based printers have the drawback of printing parts with a very low surface finish quality. This often necessitates post-machining, which in turn leads to increased material waste.

MEX offers significant flexibility for printing metal-polymer composite materials, as it allows for cost-effective adjustments to the composition of the filament feedstock. This makes it well-suited for applications like manufacturing bonded magnets, where custom geometries and material blends are important. MEX printers are generally much more affordable compared to other AM technologies due to their simpler printing mechanisms. However, compared to other 3D printing methods, MEX generally ranks in the low to middle range in terms of surface quality, printing speed, and accuracy, often requiring post-processing to improve surface finish.

D. Ongoing and Future Research Outlook

The AM of metallic components is rapidly evolving, presenting significant opportunities for the design of magnetic cores in EM application. Figure 10 illustrates the current and future key research directions in the AM of magnetic cores for EMs, along with examples that provide further clarification of the discussed topics. One key research outlook that is currently in its early stages is the selective control of the material's microstructure at the microscale. This approach potentially enables precise and localized control of anisotropic permeability, allowing the magnetic flux to be guided in specific directions within certain regions. A potential application of this concept could be in the rotor of SynRMs, where flux guides and barriers could be engineered at the microscale rather than the traditionally used macroscale. Furthermore, advancements in engineering the microstructure of printed cores could also be utilized to locally tailor the mechanical properties of high-speed rotors, strengthening regions that experience the highest stress levels.

Advanced 3D magnetic core designs, enabled by the design freedom offered by AM, is an ongoing research direction that leads to innovative EMs with enhanced performance. Additionally, this opportunity can be leveraged to implement integrated cooling systems within the active components, improving thermal performance, increasing reliability, and reducing costs. Multi-material printing is another area of AM that is under development and has the potential to enable more advanced design and manufacturing of EMs. This feature allows for the co-printing of different materials and regions, such as magnetic flux guides and barriers in SynRMs, or the co-printing of PMs and rotor cores. Such advancements can result in designs with improved mechanical strength, reduced assembly steps, and enhanced reliability. However, a current challenge in multi-material printing is the occurrence of mechanical defects and cracking in the final parts due to the

different thermal expansion coefficients of the materials used. This limitation currently restricts the selection of material pairs to those with very similar thermo-mechanical properties. More advancement in this topic requires further study on graded material transitions or advanced process monitoring.

Another recent research outlook in the 3D printing of magnetic cores is the development of recyclable magnetic cores or the utilization of recycled materials for printing magnetic cores. This approach is particularly important for rare-earth magnets, as it can lead to significant cost reductions, more stable market prices, and greater environmental benefits.

While advancements in this field are rapid, several challenges still need to be addressed. In addition to the existing challenges in achieving desirable magnetic characteristics for 3D printed magnetic cores and minimizing mechanical defects, scalability remains a significant concern. Currently, AM of magnetic cores is at the prototype stage. However, scaling AM processes for mass production requires further innovations in faster printing techniques, such as binder jetting, to enable the large-scale production of magnetic cores for industrial applications.

VI. Conclusion

This study provides a comprehensive exploration of the electromagnetic and mechanical characteristics of soft and hard magnetic cores produced using additive manufacturing (AM), particularly in the context of electrical machine applications. The commonly employed AM techniques and materials are considered for both soft and hard magnetic cores, with detailed analyses of their printing procedures, advantages, and limitations. The impact of heat treatment on the printed soft magnetic cores is also addressed, revealing a significant positive influence on the magnetic properties of printed cores. The heat treatment process notably enhances permeability while decreasing coercivity, achieved through stress relief and grain size enlargement.

The analysis of printed soft and hard magnetic cores highlights a significant influence of the chosen AM method on their multi-physics properties. This influence stems from the distinct particle bonding, melting, or sintering processes associated with each technique. When comparing various AM methods in production of soft magnetic cores, it becomes evident that cores produced with binder jetting generally exhibit noticeably inferior characteristics compared to those produced using laser powder bed fusion (LPBF) and directed energy deposition methods. The survey underscores that, in most cases, the relative permeability of printed cores are considerably lower than that of commercial laminated cores. However, the difference in saturation flux density is in general less pronounced. For 3D printing permanent magnets, NdFeB is the most extensively researched material. Analysis shows that NdFeB magnets produced through LPBF and material extrusion exhibit characteristics similar to those of commercial bonded NdFeB magnets, with LPBF offering better performance than material extrusion in general. Despite this, 3D printed NdFeB magnets are still not comparable to commercial sintered NdFeB magnets. In terms of mechanical strength, many studies have reported comparable or even superior characteristics in printed soft and hard magnetic cores. It's important to note that, despite being in its early stages, 3D printing technology shows great potential to compete with conventional manufacturing processes for producing magnetic cores with fine-tuned characteristics.

Acknowledgment

This research was supported by the European Union under the Marie Sklodowska-Curie Doctoral-Industrial project (HORIZON-MSCA-2021-DN-01), with the title “New Generation of Electrical Machines Enabled by Additive Manufacturing—EMByAM”.

Funded by
the European Union

References

[1] P. S. Ghahfarokhi *et al.*, "Opportunities and challenges of utilizing additive manufacturing approaches in thermal management of electrical machines," *IEEE Access,* vol. 9, pp. 36368-36381, 2021.

[2] R. Guschlbauer, S. Momeni, F. Osmanlic, and C. Körner, "Process development of 99.95% pure copper processed via selective electron beam melting and its mechanical and physical properties," *Materials Characterization,* vol. 143, pp. 163-170, 2018.

[3] S. J. Raab, R. Guschlbauer, M. A. Lodes, and C. Körner, "Thermal and electrical conductivity of 99.9% pure copper processed via selective electron beam melting," *Advanced Engineering Materials,* vol. 18, no. 9, pp. 1661-1666, 2016.

[4] F. Wu, A. M. EL-Refaie, and A. Al-Qarni, "Minimization of winding AC losses using inhomogeneous electrical conductivity enabled by additive manufacturing," *IEEE Transactions on Industry Applications,* vol. 58, no. 3, pp. 3447-3458, 2022.

[5] B. Lizarribar *et al.*, "Multiphysics topology optimization of aluminium and copper conductors for automotive electrical machines," *IEEE Transactions on Transportation Electrification,* 2024.

[6] Y. Yamada, H. Sugimoto, and K. Imae, "Design of High Slot Fill Aluminum Winding in a Permanent Magnet Synchronous Machine With Reduced Winding Loss," *IEEE Transactions on Industry Applications,* vol. 59, no. 2, pp. 1437-1445, 2023.

[7] A. Selema, J. Van Den Abbeele, M. N. Ibrahim, and P. Sergeant, "Innovative 3D Printed Coil and Cooling Designs for Weight-Sensitive Energy-Saving Electrical Machine," *IEEE Transactions on Transportation Electrification,* 2023.

[8] A. Thabuis, X. Ren, and Y. Perriard, "Enhanced electric motors using multi-functional 3D printed winding with integrated heat sinks," *IEEE Transactions on Energy Conversion,* vol. 38, no. 2, pp. 849-858, 2022.

[9] H. Tan *et al.*, "Additively Manufactured Winding Design for Thermal Improvement of an Oil-cooled Axial Flux Permanent Magnet Machine," *IEEE Transactions on Transportation Electrification,* vol. 10, no. 1, pp. 1911-1922, 2023.

[10] N. Simpson, G. Yiannakou, H. Felton, J. Robinson, A. Arjunan, and P. Mellor, "Direct thermal management of windings enabled by additive manufacturing," *IEEE Transactions on Industry Applications,* vol. 59, no. 2, pp. 1319-1327, 2022.

[11] F. Nishanth, A. D. Goodall, I. Todd, and E. L. Severson, "Characterization of an Axial Flux Machine with an Additively Manufactured Stator," *IEEE Transactions on Energy Conversion,* 2023.

[12] A. Selema *et al.*, "New Measurement Approach and Development of 3D-Printed Core for Yokeless Axial-Flux Machine," *IEEE Sensors Journal,* 2024.

[13] J. Krishnasamy and M. Hosek, "Spray-formed hybrid-field traction motor," SAE Technical Paper, 0148-7191, 2017.

[14] A. M. Ajamloo, M. N. Ibrahim, and P. Sergeant, "Design Considerations of a New IPM Rotor With Efficient Utilization of PMs Enabled by Additive Manufacturing," *IEEE Access,* 2024.

[15] B. Lizarribar, B. Prieto, M. Martinez-Iturralde, and G. Artetxe, "Novel topology optimization method for weight reduction in electrical machines," *IEEE Access,* vol. 10, pp. 67521-67531, 2022.

[16] M. Bieber, M. Haase, F. Tasche, A. Zibart, and B. Ponick, "Additively manufactured air-cooled lightweight rotor for an automotive electric motor," in *2023 IEEE International Electric Machines & Drives Conference (IEMDC)*, 2023: IEEE, pp. i-vii.

[17] A. Cavagnino, S. Vaschetto, E. Pošković, A. Fortunato, and E. Liverani, "Magnetic Behavior and Loss Assessment of Additively Manufactured Fe-Si alloys," in *2023 IEEE International Electric Machines & Drives Conference (IEMDC)*, 2023: IEEE, pp. 1-6.

[18] P. Klima, J. Barta, D. Koutny, and O. Vitek, "High-Speed Synchronous Reluctance Machine Rotor Using Multi-Material Additive Manufacturing," *IEEE Transactions on Energy Conversion,* 2024.

[19] D. Newman *et al.*, "Development of Solid Synchronous Reluctance Rotors With Multi-Material Additive Manufacturing," *IEEE Transactions on Industry Applications,* 2024.

[20] B. Fahimi *et al.*, "Automotive Electric Propulsion Systems: A Technology Outlook," *IEEE Transactions on Transportation Electrification,* 2023.

[21] X. Tao and P. Huiqing, "Formation cause, composition analysis and comprehensive utilization of rare earth solid wastes," *Journal of rare earths,* vol. 27, no. 6, pp. 1096-1102, 2009.

[22] K. Gandha, G. Ouyang, S. Gupta, V. Kunc, M. P. Paranthaman, and I. C. Nlebedim, "Recycling of additively printed rare-earth bonded magnets," *Waste Management,* vol. 90, pp. 94-99, 2019.

[23] M. A. Rosa *et al.*, "Using Recycled Nanocrystalline HDDR Powders in the Additive Manufacturing of Bonded Nd-Fe-B Magnets," *IEEE Transactions on Magnetics,* 2024.

[24] J. Jacimovic *et al.*, "Net shape 3D printed NdFeB permanent magnet," *arXiv preprint arXiv:1611.05332,* 2016.

[25] S. Singh *et al.*, "Cold-spray additive manufacturing of a petal-shaped surface permanent magnet traction motor," *IEEE Transactions on Transportation Electrification,* vol. 9, no. 3, pp. 3636-3648, 2023.

[26] T. Mukherjee *et al.*, "Control of grain structure, phases, and defects in additive manufacturing of high-performance metallic components," *Progress in Materials Science,* vol. 138, p. 101153, 2023.

[27] S. Gao *et al.*, "Additive manufacturing of alloys with programmable microstructure and properties," *Nature Communications,* vol. 14, no. 1, p. 6752, 2023.

[28] A. M. Ajamloo, M. N. Ibrahim, and P. Sergeant, "A Review on Properties of 3D Printed Magnetic Cores for Electrical Machines: Additive Manufacturing Methods and Materials," in *2024 International Conference on Electrical Machines (ICEM)*, 2024: IEEE, pp. 01-07.

[29] D. Goll *et al.*, "Additive manufacturing of soft magnetic materials and components," *Additive Manufacturing,* vol. 27, pp. 428-439, 2019.

[30] A. Selema *et al.*, "Evaluation of 3d-Printed Magnetic Materials for Additively-Manufactured Electrical Machines," *Journal of Magnetism and Magnetic Materials,* vol. 569, p. 170426, 2023.

[31] X. Shen *et al.*, "Evaluation of microstructure, mechanical and magnetic properties of laser powder bed fused Fe-Si alloy for 3D magnetic flux motor application," *Materials & Design,* vol. 234, p. 112343, 2023.

[32] B. Koo *et al.*, "Structurally-layered soft magnetic Fe-Si components with surface insulation prepared by shell-shaping selective laser melting," *Applied Surface Science,* vol. 553, p. 149510, 2021.

[33] H. Tiismus *et al.*, "Laser Additively Manufactured Magnetic Core Design and Process for Electrical Machine Applications," *Energies,* vol. 15, no. 10, p. 3665, 2022.

[34] H. Tiismus *et al.*, "AC magnetic loss reduction of SLM processed Fe-Si for additive manufacturing of electrical machines," *Energies,* vol. 14, no. 5, p. 1241, 2021.

[35] A. B. Kustas *et al.*, "Characterization of the Fe-Co-1.5 V soft ferromagnetic alloy processed by Laser Engineered Net Shaping (LENS)," *Additive Manufacturing,* vol. 21, pp. 41-52, 2018.

[36] S. Li *et al.*, "3D printing of ductile equiatomic Fe-Co alloy for soft magnetic applications," *Additive Manufacturing,* vol. 47, p. 102291, 2021.

[37] K. A. Liogas *et al.*, "Effect of heat treatment on the microstructure and magnetic properties of laser powder bed fusion processed equiatomic Co-Fe," *Additive Manufacturing,* vol. 67, p. 103499, 2023.

[38] T. Riipinen, S. Metsä-Kortelainen, T. Lindroos, J. S. Keränen, A. Manninen, and J. Pippuri-Mäkeläinen, "Properties of soft magnetic Fe-Co-V alloy produced by laser powder bed fusion," *Rapid Prototyping Journal,* vol. 25, no. 4, pp. 699-707, 2019.

[39] M. Garibaldi, I. Ashcroft, J. Lemke, M. Simonelli, and R. Hague, "Effect of annealing on the microstructure and magnetic properties of soft magnetic Fe-Si produced via laser additive manufacturing," *Scripta Materialia,* vol. 142, pp. 121-125, 2018.

[40] D. Michieletto, L. Alberti, F. Zanini, and S. Carmignato, "Electromagnetic Characterization of Silicon–Iron Additively Manufactured Cores for Electric Machines," *Energies,* vol. 17, no. 3, p. 650, 2024.

[41] H. Lee *et al.*, "Effect of process parameters on the texture evolution of Fe-6.5 wt% Si soft magnetic alloys manufactured via laser powder bed fusion," *Journal of Materials Processing Technology,* vol. 331, p. 118521, 2024.

[42] B. Kocsis, M. Windisch, I. Mészáros, and L. K. Varga, "3D printing parameters optimization for Fe-6.5 wt% Si," *Journal of Magnetism and Magnetic Materials,* vol. 592, p. 171829, 2024.

[43] J. S. Corporation. "Super Core." https://www.jfe-steel.co.jp/en/products/electrical/catalog/f1e-002.pdf (accessed Online).

[44] J. S. Corporation. "Electrical Steel Sheets." https://www.jfe-steel.co.jp/en/products/electrical/catalog/f1e-001.pdf (accessed Online).

[45] S. Urbanek, *Gestaltung von Rotoren permanentmagneterregter Synchronmaschinen für die Metalladditive Fertigung*. Garbsen/Hannover: TEWISS Verlag, 2021.

[46] M. Stella, V. Bertolini, F. R. Fulginei, A. Di Schino, and A. Faba, "Experimental Measurements and Numerical Computations of a Ferromagnetic Core Made by Means of Additive Manufacturing," in *IEEE EUROCON 2023-20th International Conference on Smart Technologies*, 2023: IEEE, pp. 423-428.

[47] H. Tiismus, A. Kallaste, T. Vaimann, A. Rassõlkin, and A. Belahcen, "Additive manufacturing of prototype axial flux switched reluctance electrical machine," in *2021 28th International Workshop on Electric Drives: Improving Reliability of Electric Drives (IWED)*, 2021: IEEE, pp. 1-4.

[48] Y. Zhou *et al.*, "Design of an Axial-Flux Synchronous Reluctance Machine with 3D-Printed Rotor," in *2023 IEEE International Electric Machines & Drives Conference (IEMDC)*, 2023: IEEE, pp. 1-7.

[49] H. Tiismus, A. Kallaste, M. U. Naseer, T. Vaimann, and A. Rassõlkin, "Design and Performance of Laser Additively Manufactured Core Induction Motor," *IEEE Access,* vol. 10, pp. 50137-50152, 2022.

[50] H. Tiismus, A. Kallaste, A. Belahcen, A. Rassolkin, T. Vaimann, and P. Shams Ghahfarokhi, "Additive manufacturing and performance of E-type transformer core," *Energies,* vol. 14, no. 11, p. 3278, 2021.

[51] S. Gao, "Additive manufacturing Processing and characterization of Fe-Si soft magnetic alloys," Bourgogne Franche-Comté, 2021.

[52] M. Zaied, A. Ospina-Vargas, N. Buiron, J. Favergeon, and N.-E. Fenineche, "Additive Manufacturing of Soft Ferromagnetic Fe 6.5% Si Annular Cores: Process Parameters, Microstructure, and Magnetic Properties," *IEEE Transactions on Magnetics,* vol. 58, no. 11, pp. 1-9, 2022.

[53] L. Jiang *et al.*, "Influence of annealing treatment on grain growth, texture and magnetic properties of a selective laser melted Fe-6.5 wt% Si alloy," *Journal of Materials Research and Technology,* vol. 32, pp. 1324-1341, 2024.

[54] M. Garibaldi, I. Ashcroft, N. Hillier, S. Harmon, and R. Hague, "Relationship between laser energy input, microstructures and magnetic properties of selective laser melted Fe-6.9% wt Si soft magnets," *Materials Characterization,* vol. 143, pp. 144-151, 2018.

[55] A. Manninen, J. Pippuri-Mäkeläinen, T. Riipinen, T. Lindroos, S. Metsä-Kortelainen, and A. Antikainen, "The Mitigation of Eddy-Current Losses in Ferromagnetic Samples Produced by Laser Powder Bed Fusion," *IEEE Access,* vol. 10, pp. 115571-115582, 2022.

[56] T. Lindroos, T. Riipinen, S. Metsä-Kortelainen, J. Pippuri-Mäkeläinen, and A. Manninen, "Lessons learnt-additive manufacturing of iron cobalt based soft magnetic materials," *Journal of Magnetism and Magnetic Materials,* vol. 563, p. 169977, 2022.

[57] S. Metsä-Kortelainen *et al.*, "Manufacturing of topology optimized soft magnetic core through 3D printing," in *NAFEMS Exploring the Design Freedom of Additive Manufacturing through Simulation*, 2016.

[58] C. Electrification. "Hiperco 50A." https://www.carpenterelectrification.com/hiperco-50a-datasheet (accessed Online).

[59] J. Laine, K. Jalava, J. Vaara, K. Soivio, T. Frondelius, and J. Orkas, "The mechanical properties of ductile iron at intermediate

temperatures: the effect of silicon content and pearlite fraction," *International Journal of Metalcasting,* vol. 15, pp. 538-547, 2021.
[60] C. L. Cramer *et al.*, "Binder jet additive manufacturing method to fabricate near net shape crack-free highly dense Fe-6.5 wt.% Si soft magnets," *Heliyon,* vol. 5, no. 11, 2019.
[61] T. Q. Pham, T. T. Do, P. Kwon, and S. N. Foster, "Additive manufacturing of high performance ferromagnetic materials," in *2018 IEEE Energy Conversion Congress and Exposition (ECCE)*, 2018: IEEE, pp. 4303-4308.
[62] T. Q. Pham *et al.*, "Binder jet printed iron silicon with low hysteresis loss," in *2019 IEEE International Electric Machines & Drives Conference (IEMDC)*, 2019: IEEE, pp. 1045-1052.
[63] B. Khoshoo, K. J. Islam, H. Suen, P. Kwon, J. P. Lozano, and S. N. Foster, "Eddy Current Loss Reduction in Binder Jet Printed Iron Silicon Cores," in *2022 International Conference on Electrical Machines (ICEM)*, 2022: IEEE, pp. 558-564.
[64] S. Firdosy *et al.*, "Processing–Microstructure–Property Relationships in a Laser-Deposited Fe-Co-V Alloy," *Advanced Engineering Materials,* vol. 24, no. 4, p. 2100931, 2022.
[65] T. F. Babuska *et al.*, "Achieving high strength and ductility in traditionally brittle soft magnetic intermetallics via additive manufacturing," *Acta Materialia,* vol. 180, pp. 149-157, 2019.
[66] M. Nartu *et al.*, "Reducing coercivity by chemical ordering in additively manufactured soft magnetic Fe–Co (Hiperco) alloys," *Journal of Alloys and Compounds,* vol. 861, p. 157998, 2021.
[67] T. Q. Pham, H. Suen, P. Kwon, G. Kumari, C. J. Boehlert, and S. N. Foster, "Reduction in hysteresis loss of binder jet printed iron silicon with boron," *IEEE Transactions on Industry Applications,* vol. 57, no. 5, pp. 4864-4873, 2021.
[68] G. Kumari *et al.*, "Improving the soft magnetic properties of binder jet printed iron-silicon alloy through boron addition," *Materials Chemistry and Physics,* vol. 296, p. 127181, 2023.
[69] A. Y. Kumar, Y. Bai, A. Eklund, and C. B. Williams, "The effects of Hot Isostatic Pressing on parts fabricated by binder jetting additive manufacturing," *Additive Manufacturing,* vol. 24, pp. 115-124, 2018.
[70] V. Chaudhary *et al.*, "Additive manufacturing of functionally graded Co–Fe and Ni–Fe magnetic materials," *Journal of Alloys and Compounds,* vol. 823, p. 153817, 2020.
[71] K. Gandha *et al.*, "Additive manufacturing of anisotropic hybrid NdFeB-SmFeN nylon composite bonded magnets," *Journal of Magnetism and Magnetic Materials,* vol. 467, pp. 8-13, 2018.
[72] B. Yao, X. Lin, X. Lu, Z. Li, X. Li, and H. Yang, "An effective laser in-situ re-scanning strategy in laser powder bed fusion of Nd-Fe-B permanent magnets: Crack reduction and magnetic properties enhancement," *Additive Manufacturing,* vol. 90, p. 104311, 2024.
[73] F. Bittner, A. K. Putta, F. Juerries, T. G. Woodcock, W.-G. Drossel, and J. Thielsch, "The impact of post-processing heat treatment on the magnetic properties of additively manufactured Nd-Fe-B magnets," *Journal of Magnetism and Magnetic Materials,* p. 172238, 2024.
[74] D. Goll, F. Trauter, T. Bernthaler, J. Schanz, H. Riegel, and G. Schneider, "Additive manufacturing of bulk nanocrystalline FeNdB based permanent magnets," *Micromachines,* vol. 12, no. 5, p. 538, 2021.
[75] J. Slapnik, I. Pulko, R. Rudolf, I. Anžel, and M. Brunčko, "Fused filament fabrication of Nd-Fe-B bonded magnets: Comparison of PA12 and TPU matrices," *Additive Manufacturing,* vol. 38, p. 101745, 2021.
[76] A. Baldissera, P. Pavez, P. Wendhausen, C. Ahrens, and J. Mascheroni, "Additive manufacturing of bonded Nd–Fe–B—Effect of process parameters on magnetic properties," *IEEE Transactions on Magnetics,* vol. 53, no. 11, pp. 1-4, 2017.
[77] R. Fim, A. Mascheroni, L. Antunes, J. Engerroff, C. Ahrens, and P. Wendhausen, "Increasing packing density of Additively Manufactured Nd-Fe-B bonded magnets," *Additive Manufacturing,* vol. 35, p. 101353, 2020.
[78] N. Urban, A. Meyer, S. Kreitlein, F. Leicht, and J. Franke, "Efficient near net-shape production of high energy rare earth magnets by laser beam melting," *Applied Mechanics and Materials,* vol. 871, pp. 137-144, 2017.
[79] M. Skalon *et al.*, "Influence of melt-pool stability in 3D printing of NdFeB magnets on density and magnetic properties," *Materials,* vol. 13, no. 1, p. 139, 2019.
[80] O. Tosoni *et al.*, "High-coercivity copper-rich Nd-Fe-B magnets by powder bed fusion using laser beam method," *Additive Manufacturing,* vol. 64, p. 103426, 2023.
[81] J. Wu *et al.*, "Additive manufacturing of Nd-Fe-B permanent magnets and their application in electrical machines," *IEEE Access,* 2024.
[82] B. G. Compton *et al.*, "Direct-write 3D printing of NdFeB bonded magnets," *Materials and Manufacturing Processes,* vol. 33, no. 1, pp. 109-113, 2018.
[83] A. Shen, C. P. Bailey, A. W. Ma, and S. Dardona, "UV-assisted direct write of polymer-bonded magnets," *Journal of Magnetism and Magnetic Materials,* vol. 462, pp. 220-225, 2018.
[84] M. P. Paranthaman *et al.*, "Additive manufacturing of isotropic NdFeB PPS bonded permanent magnets," *Materials,* vol. 13, no. 15, p. 3319, 2020.
[85] L. Li *et al.*, "Big area additive manufacturing of high performance bonded NdFeB magnets," *Scientific reports,* vol. 6, no. 1, pp. 1-7, 2016.
[86] L. Li *et al.*, "Fabrication of highly dense isotropic Nd-Fe-B nylon bonded magnets via extrusion-based additive manufacturing," *Additive Manufacturing,* vol. 21, pp. 495-500, 2018.
[87] M. P. Paranthaman *et al.*, "Binder jetting: A novel NdFeB bonded magnet fabrication process," *Jom,* vol. 68, pp. 1978-1982, 2016.
[88] L. Li *et al.*, "A novel method combining additive manufacturing and alloy infiltration for NdFeB bonded magnet fabrication," *Journal of Magnetism and Magnetic Materials,* vol. 438, pp. 163-167, 2017.
[89] F. Bernier and J. Lamarre, "Metal-NdFeB composite permanent magnets produced by cold spray," in *29th International Electric Vehicle Symposium*, 2016.
[90] J.-M. Lamarre and F. Bernier, "Permanent magnets produced by cold spray additive manufacturing for electric engines," *Journal of Thermal Spray Technology,* vol. 28, pp. 1709-1717, 2019.
[91] BOMATEC. "Plastic-bonded NdFeB magnets." https://www.bomatec.com/en/products/magnets/plastic-bonded-ndfeb-magnets#data (accessed Online).
[92] A. M. Technologies. "Injection Molded Magnets." https://www.arnoldmagnetics.com/wp-content/uploads/2017/10/Arnold-BMG-Magnet-Material-Specification-Brochure.pdf (accessed Online).
[93] B. Magnetics. "Neodymium Sintered - Standard Grades." https://bakkermagnetics.com/wp-content/uploads/2019/01/neodymium_sintered_-_standard_grades_0.pdf (accessed Online).
[94] C. Huber, S. Cano, I. Teliban, S. Schuschnigg, M. Groenefeld, and D. Suess, "Polymer-bonded anisotropic SrFe12O19 filaments for fused filament fabrication," *Journal of applied physics,* vol. 127, no. 6, 2020.
[95] K. Sonnleitner *et al.*, "3D printing of polymer-bonded anisotropic magnets in an external magnetic field and by a modified production process," *Applied Physics Letters,* vol. 116, no. 9, 2020.
[96] G. Zhang *et al.*, "4D printing of the ferrite permanent magnet BaFe12O19 and its intelligent shape memory effect," *Journal of Alloys and Compounds,* p. 176307, 2024.
[97] F. Yang, X. Zhang, Z. Guo, and A. A. Volinsky, "3D gel-printing of Sr ferrite parts," *Ceramics International,* vol. 44, no. 18, pp. 22370-22377, 2018.
[98] E. Magnetics. "Ferrite Magnets/Ceramic Magnets Datasheet." https://www.eclipsemagnetics.com/site/assets/files/19602/ferrite_ceramic_datasheet.pdf (accessed Online).
[99] E. White *et al.*, "Processing of alnico magnets by additive manufacturing," *Applied Sciences,* vol. 9, no. 22, p. 4843, 2019.
[100] Z.-Y. Zhang *et al.*, "High-performance Alnico magnets prepared by powder bed fusion," *Journal of Alloys and Compounds,* vol. 976, p. 173380, 2024.
[101] E. M. H. White, A. G. Kassen, E. Simsek, W. Tang, R. T. Ott, and I. E. Anderson, "Net shape processing of alnico magnets by additive manufacturing," *IEEE Transactions on Magnetics,* vol. 53, no. 11, pp. 1-6, 2017.
[102] Bunting—Berkhamsted. "Alnico Magnets Datasheet." https://www.bunting-berkhamsted.com/wp-content/uploads/2019/11/Bunting-Alnico-Magnets-Data-Sheet.pdf (accessed Online).
[103] C. Huber *et al.*, "Coercivity enhancement of selective laser sintered NdFeB magnets by grain boundary infiltration," *Acta Materialia,* vol. 172, pp. 66-71, 2019.
[104] P. Wendhausen, C. Ahrens, A. Baldissera, P. Pavez, and J. Mascheroni, "Additive manufacturing of bonded NdFeB, process parameters evaluation on magnetic properties," in *2017 IEEE International Magnetics Conference (INTERMAG)*, 2017: IEEE, pp. 1-1.

[105] C. Huber, G. Mitteramskogler, M. Goertler, I. Teliban, M. Groenefeld, and D. Suess, "Additive manufactured polymer-bonded isotropic NdFeB magnets by stereolithography and their comparison to fused filament fabricated and selective laser sintered magnets," *Materials,* vol. 13, no. 8, p. 1916, 2020.
[106] J. Wu, N. T. Aboulkhair, M. Degano, I. Ashcroft, and R. J. Hague, "Process-structure-property relationships in laser powder bed fusion of permanent magnetic Nd-Fe-B," *Materials & Design,* vol. 209, p. 109992, 2021.
[107] F. Bittner, J. Thielsch, and W.-G. Drossel, "Microstructure and magnetic properties of Nd-Fe-B permanent magnets produced by laser powder bed fusion," *Scripta Materialia,* vol. 201, p. 113921, 2021.
[108] K. Schäfer, T. Braun, S. Riegg, J. Musekamp, and O. Gutfleisch, "Polymer-bonded magnets produced by laser powder bed fusion: Influence of powder morphology, filler fraction and energy input on the magnetic and mechanical properties," *Materials Research Bulletin,* vol. 158, p. 112051, 2023.
[109] H.-J. Kim *et al.*, "Microstructural investigation of nanocrystalline Nd-Fe-B magnets fabricated by laser powder bed fusion," *Materials Characterization,* vol. 216, p. 114228, 2024.
[110] M. Mapley, J. P. Pauls, G. Tansley, A. Busch, and S. D. Gregory, "Selective laser sintering of bonded magnets from flake and spherical powders," *Scripta Materialia,* vol. 172, pp. 154-158, 2019.
[111] C. Huber *et al.*, "3D print of polymer bonded rare-earth magnets, and 3D magnetic field scanning with an end-user 3D printer," *Applied Physics Letters,* vol. 109, no. 16, 2016.
[112] C. Huber *et al.*, "3D printing of polymer-bonded rare-earth magnets with a variable magnetic compound fraction for a predefined stray field," *Scientific reports,* vol. 7, no. 1, p. 9419, 2017.
[113] K. von Petersdorff-Campen *et al.*, "3D printing of functional assemblies with integrated polymer-bonded magnets demonstrated with a prototype of a rotary blood pump," *Applied Sciences,* vol. 8, no. 8, p. 1275, 2018.
[114] S. Dussa, S. S. Joshi, M. Radhakrishnan, K. M. Krishna, and N. B. Dahotre, "Laser directed energy deposition of Alnico-8H from blended elemental powders: Effect of nickel increase on magnetic properties," *Journal of Magnetism and Magnetic Materials,* p. 172490, 2024.
[115] D. Systems. "DMP Flex 100." https://www.3dsystems.com/3d-printers/dmp-flex-100 (accessed Online).
[116] X. Metal. "The XM200G Printer." https://xactmetal.com/xm200g-2/ (accessed Online).
[117] HBD. "HBD 1000Pro." https://en.hb3dp.com/product/48.html (accessed Online).
[118] N. SLM. "SLM 125." https://www.slm-solutions.com/products-and-solutions/machines/slm-125/ (accessed Online).
[119] N. SLM. "SLM 500." https://www.slm-solutions.com/products-and-solutions/machines/slm-500/ (accessed Online).
[120] AddUp. "FormUp 350: The Benchmark in Reliable, Repeatable, and Industrial L-PBF Machines." https://addupsolutions.com/machines/pbf/formup-350/ (accessed Online).
[121] P. Additive. "Additive Manufacturing turnkey solutions." https://www.primaadditive.com/files/primaadditive/attachments/Prima_Additive_Catalogo_11-23_WEB.pdf (accessed.
[122] Markforged. "PX100, Additive metal production at unmatched precision. The next generation of Digital Metal." https://markforged.com/3d-printers/px100 (accessed Online).
[123] HP. "HP Metal Jet S100 3D Printing Solution." https://www.hp.com/us-en/printers/3d-printers/products/metal-jet.html (accessed Online).
[124] D. Metal. "X-Series." https://www.desktopmetal.com/products/xseries (accessed Online).
[125] D. Metal. "Production System." https://www.desktopmetal.com/products/production (accessed Online).
[126] Meltio. "Meltio M450 Turn-key Metal 3D Printer." https://meltio3d.com/metal-3d-printers/meltio-m450/ (accessed Online).
[127] AddUp. "AddUp's Modulo 400: The Future of Industrial DED Machines." https://addupsolutions.com/machines/ded/modulo-400/ (accessed.
[128] AddUp. "Magic 800 DED Machine: A Revolution in High-Volume, High-Power Industrial Production." https://addupsolutions.com/machines/ded/magic-800/ (accessed Online).
[129] ADDITEC. "Introducing the AMDROiD: A Revolutionary Laser-Wire DED System." https://additec3d.com/amdroid-6/ (accessed Online).
[130] Markforged. "Metal X System." https://markforged.com/3d-printers/metal-x (accessed Online).
[131] Raise3D. "Raise3D Forge1 – The Metal FFF 3D Printer." https://www.raise3d.com/raise3d-forge1-a-metal-fff-3d-printer/ (accessed Online).
[132] D. Metal. "Studio System 2." https://www.desktopmetal.com/products/studio (accessed Online).
[133] S. S. G. AG. "SLM 280." https://slm280.slm-solutions.com/ (accessed Online).

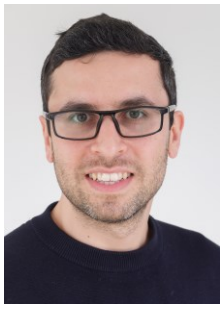

Akbar Mohammadi Ajamloo received the B.Sc. degree in Electrical Engineering in 2016 and the M.Sc. degree in Electrical Machines and Power Electronics in 2018, both from K.N. Toosi University of Technology, Tehran, Iran. He is currently pursuing the PhD degree with the Department of Electromechanical, Systems and Metal Engineering at Ghent University, Gent, Belgium. His research interests include advanced topologies, multi-physics analysis, optimization and analytical modelling of electrical machines. He is also actively involved in the additive manufacturing of electromagnetic components for industrial and sustainable energy applications.

Mohamed N. Ibrahim received the M.Sc. degree in electrical power and machines engineering from Tanta University, Egypt in November 2012, and the Ph.D. degree in electromechanical engineering from Ghent University, Belgium in December 2017. In November 2008 and April 2018, he became a Teaching Assistant and an Assistant Professor (on leave) respectively at Electrical Engineering Department, Kafrelshiekh University, Egypt and since August 2023 he is an Associate Professor (on leave). Since December 2017, Dr. Ibrahim is working as a Post-Doctoral researcher with the Department of Electromechanical, Systems and Metal Engineering, Ghent University, Belgium. He is also an Affiliate Member of Flanders Make, the strategic research center for the manufacturing industry in Flanders, Belgium. His research interest focuses on electrical machines and drives for sustainability. He has over 100 publications and 1 patent in this research field. He is a senior Member of the IEEE. Dr. Ibrahim was a recipient of several times the Kafrelshiekh University Award for his international scientific publications. He serves as an Associate editor for IEEE Transactions on Magnetics and as a Guest Editor for Energies, Mathematics and Electronics journals. Also, he is a Reviewer for several journals and conferences including IEEE Transactions, etc.

Peter Sergeant (senior member IEEE) received the master's degree in electromechanical engineering in 2001, and the Ph.D. degree in electromechanical engineering in 2006, both from Ghent University, Ghent, Belgium. In 2006 and 2012, he became a postdoctoral researcher and associate professor respectively. Since 2022, he is full professor at Ghent University. His research domain is electrical machines and drives for industrial, automotive and sustainable energy applications. The focus is on accurate modeling, prototyping and testing of machines and drives, for improving reliability, sustainability, energy efficiency and power density.